Development of Intelligent Electroprocessing Technology for Nickel-based Superalloy Special-shaped Electrodes

Yu-Ting Lyu,[1] Thi-Xuyen Bui,[2,3] Herchang Ay,[1*]
Te-Hua Fang,[2,4**] and Min-Chun Chuang[5,6]

[1]Department of Mold and Die Engineering, National Kaohsiung University of Science and Technology,
Kaohsiung 807, Taiwan
[2]Department of Mechanical Engineering, National Kaohsiung University of Science and Technology,
Kaohsiung 807, Taiwan
[3]University of Technology and Education - The University of Danang, Danang 551580, Vietnam
[4]Department of Fragrance and Cosmetic Science, Kaohsiung Medical University, Kaohsiung 807, Taiwan
[5]Department of Mechanical and Electro-Mechanical Engineering, National Sun Yat-sen University,
Kaohsiung 804, Taiwan
[6]Metal Industries Research and Development Centre (MIRDC), Kaohsiung 811, Taiwan

In this work, we designed a novel cross-process matching method and technology through sensing signals and dimensional fitting. Specifically, we mixed the electrochemical machining and sinking electrical discharge machining methods with intelligently designed special-shaped electrodes to effectively enable virtual measurement and dimension maintenance by developing intelligent electrode-processing technology for nickel-based superalloy special-shaped electrodes. The technique can help directly adjust the product accuracy of special-shaped holes on the basis of the relationship between the amount of material removed and the current by revealing errors across processing, obtaining feedback, and maintaining accuracy through matching methods without offline measurement. With a lot of time and design adjustment parameters, this method can provide more accurate and faster results than the traditional method. The electrode wear after 17 h of continuous processing is ≤10%. Processing accuracy control during discharge is ≤±0.5 μm. The processing time of the rough/medium machining process is ≤24 h, which is an increase of ≥40%. Moreover, the electrical machining process optimization improved aerospace diffuser processing efficiency by 30%.

1. Introduction

The Ni-based alloy has a number of outstanding properties such as attractive strength, oxidation resistance at high temperatures, gas corrosion resistance,[1–5] resistance to high-temperature fatigue, and free of creep;[6–8] it is highly attractive for aerospace engine applications (accounting for about 50 wt% of materials used in an aerospace engine)[9] and industrial gas

---

turbine blades, and as part of jet engines with a high-temperature strength of 1000 °C.[10–12] Nickel-based superalloy components are designed as additives manufactured for aerospace applications and are independently developed into vehicles to strengthen aerospace parts' processing and postprocessing technologies.[13–15] The Nickel-based alloy is viable for long periods of high-temperature exposure to oxidative environments and high-pressure turbine applications.[16]

Electrochemical machining (ECM) is a unique manufacturing method that operates through anodic dissolution, in which material removal appears at an ionic level. In this manufacturing process, the workpiece functions as the anode and the tool as the cathode, and the flow of a compatible electrolyte solution creates an electrolytic cell. According to Faraday's law of electrolysis, material removal occurs when a stable voltage is put between the workpiece and the tool electrode.[17–19] Moreover, ECM is an economical and effective technique for cutting high-strength, heat-resistant materials with convoluted shapes without causing mechanical distortion, compressive stresses, cracks, or thermal distortion.[20–22] However, this technique is affected by the hydrodynamic instability of the anode boundary layer due to the surface roughness.[23]

Sinking electrical discharge machining (EDM) operates by repetitive electric sparks in the electrode region that usually acts as a cathode, and the workpiece usually acts as an anode.[24–27] EDM can be applied to a complicated geometry with precise tolerance and reproducibility in hard materials.[28–31] It meets the stringent requirements in high-tech industries such as aerospace, automotive, die and mold, medical, and electronics industries.[32–36] It still has many difficulties in precisely predicting the properties of machined surfaces based on discharge parameters. At the beginning of the EDM technique development, the EDM process produced toxic pollutants because of the release of hydrocarbon and mineral dielectric liquids.[37,38] However, many researchers have successfully found eco-friendly machining techniques to protect the living environment. By increasing the use of natural resources and reducing the use of hazardous liquid dielectric fluids, Boopathi *et al.* have enhanced EDM's ecological research activities.[39] Alternatively, changing the traditional mineral dielectric liquids to pure air or gas as dielectric fluids helps to reduce the amount of debris and environmental impact and improve the results of near-dry EDM.[40–42]

In this study, we used technology integration to supplement the information required for the digitalization and intelligence of the aerospace industry to enable original equipment manufacture (OEM) with the transformation to upgrade to the field of high-value-added metal product processing. We mixed the ECM and EDM methods with intelligently designed special-shaped electrodes to effectively enable virtual measurement and dimension maintenance. This plan is based on the process requirements of EVA Aerospace's end customers.

2. Methodology

The process accuracy monitoring system used includes electrochemical processing equipment and storage and processing units. Electrochemical processing equipment is used to perform electrochemical processing on the workpiece. The storage unit is used to store the linear regression model. The processing unit is coupled to the electrochemical processing equipment

and the storage unit. The processing unit detects the operating voltage and current of the ECM equipment during the ECM process and applies the linear regression model. The processing unit inputs the working voltage and current into the linear regression model so that the linear regression model estimates the processing quality parameters of the workpiece.

To achieve high-accuracy machining, we designed a precision composite electrical machining matching process, as shown in Fig. 1. The current in the designed ECDM machine is estimated using Eqs. (1)–(3),[43] where I_{ECM} is the current of the electrochemical process, I_{ECM} is the current of the discharge process, H is the width of the electrode tool, b is the electrode tool length, v is the electrode feed rate, A_{ECM} is the electrochemical dissolution surface, k_{ECM} is the factor that estimates the electrochemical dissolution rate, and k_{EDM} is the spark factor of EDM.

$$I_{ECM} = A_{ECM} \frac{v_f}{k_{ECM}} \tag{1}$$

$$I_{EDM} = A_{EDM} \frac{v_f}{k_{EDM}} = \left(Hb - A_{ECM} \right) \frac{v_f}{k_{EDM}} \tag{2}$$

The total amount of material removed can be regarded as the total current (I_{total}) of the electrochemical and EDM currents.

$$I_{total} = I_{ECM} - I_{EDM} \tag{3}$$

To estimate the amount of material removed during the connection between two processes, the initial material (before processing) is defined as x_i, the amount removed by the ECM process is described as A_{ECM}, and the volume after processing by the EDM process is defined as x_d.

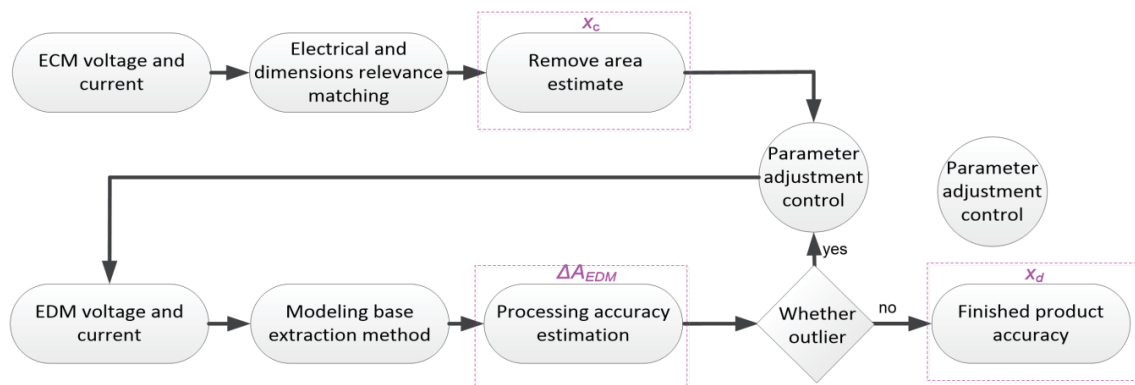$$x_c = x_i - A_{ECM} = x_i - I_{ECM} \frac{k_{ECM}}{v_f} \tag{4}$$

Fig. 1.   (Color online) Precision composite electrical machining matching process.

$$x_d = x_c - A_{EDM} = x_c - I_{EDM} \frac{k_{EDM}}{v_f} \tag{5}$$

Equations (3)–(5) show a proportional relationship between the current and the amount of material removed. They illustrate that even if I_{ECM} rises, x_c will decrease. To ensure the final x_d accuracy, the current value of I_{EDM} can be adjusted according to changes in x_c.

In terms of actual control, to achieve precise composite electrical machining matching technology, the voltage and current of ECM and EDM are collected, respectively. The electrical signals and dimensions are fitted through the machine learning model, the errors of the two processes are matched simultaneously, and feedback is provided.

3   Results and Discussion

In this work, we concentrated on optimizing the electrochemical processing of special-shaped holes in diffusion grooves to enhance the electrode lifespan. Figure 2(a) shows the outlet hole of the water of the electrode processed by drilling, which can reduce processing costs. However, its flow field distribution indicates that there is eddy current distribution between the water outlets, which makes it difficult for the processing products to be discharged, causing short circuits and reducing the lifespan of the electrodes, as shown in Fig. 2(b). Figure 2(c) shows
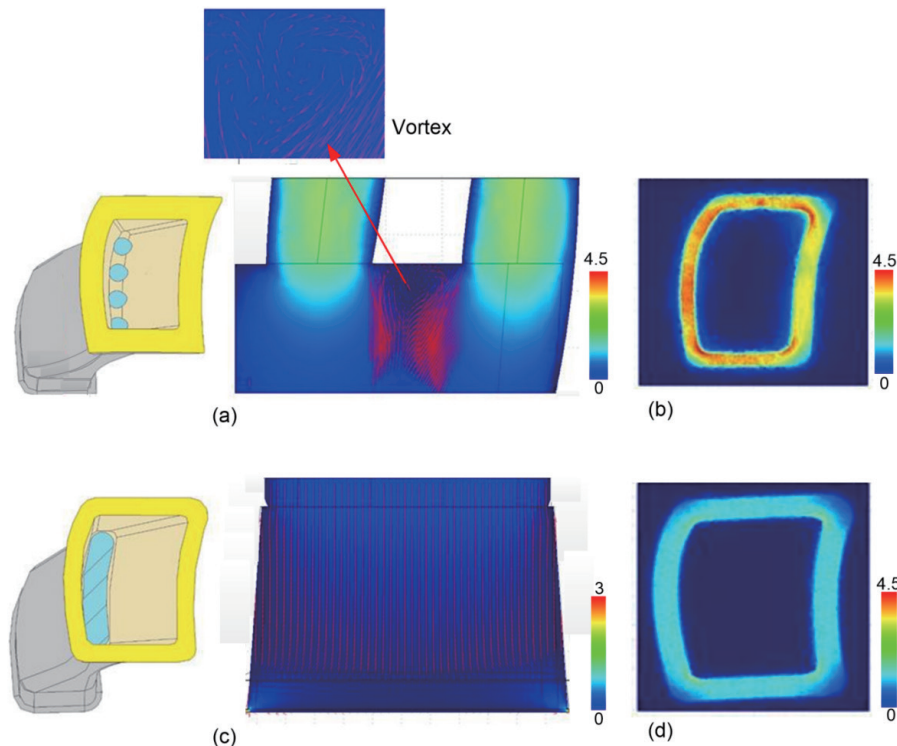

Fig. 2.   (Color online) Water outlet and flow field distribution of the electrode model: (a, b) traditional and (c, d) special-shaped electrode models.

that the water outlet hole is changed into a water outlet model, which must be processed with special tools or EDM, increasing the electrode production cost. Figure 2(c) also shows that the water outlet does not exist in the distribution of eddy currents, which improves the unstable flow field condition in the traditional electrode model in Fig. 2(a). When the electrolyte is discharged from the electrode's processed surface, the flow field's distribution can be referred to in Figs. 2(b) and 2(d). Figure 2(b) shows that the flow field does not readily have good flow velocity distribution at the four corners of the electrode surface, so it is a reasonable design to round the four corners of the electrode surface. It can also be found from Fig. 2(d) that after the overall design of the electrode is optimized, the flow rate on the electrode surface becomes even. After actual lifespan testing, the optimized electrode design has markedly improved the electrode's service life.

Since the diffusion groove channel is not a simple straight channel, an interference check of the entire electrode must be carried out through the planned processing route after completing the design. The path traveled by the electrode surface forms a thin layer, as shown in Fig. 3(a). The correct processing path must not interfere with the diffusion groove channel, and the electrode body must not interfere with the thin shell. The measurement position of the diffusion groove is shown in Fig. 3(b). The cross section taken is the AE–AE cross section, as shown in Fig. 3(c), and other measurement cross sections are taken parallel to AE–AE cross sections, as shown in Fig. 4(b).
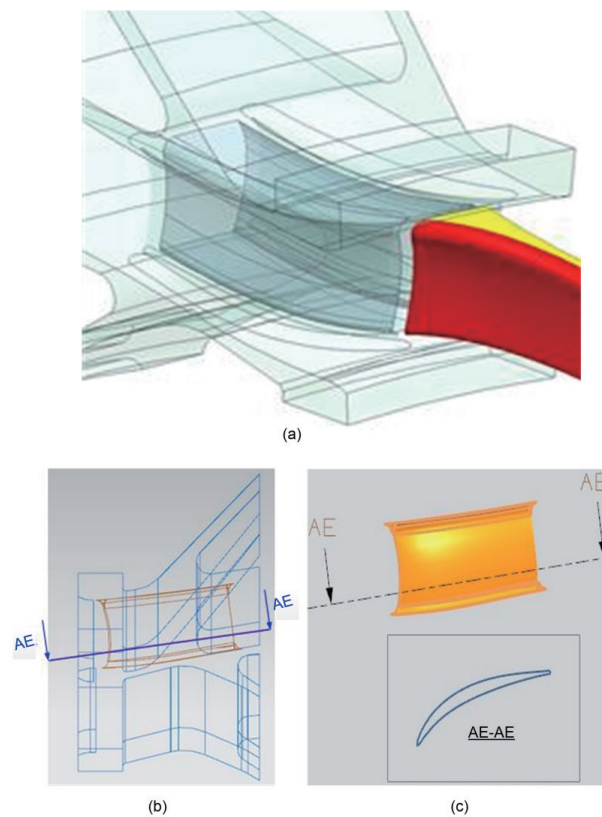

Fig. 3.   (Color online) (a) Electrode path and interference, (b) measurement position of the diffusion groove, and (c) cross section of the diffusion groove.
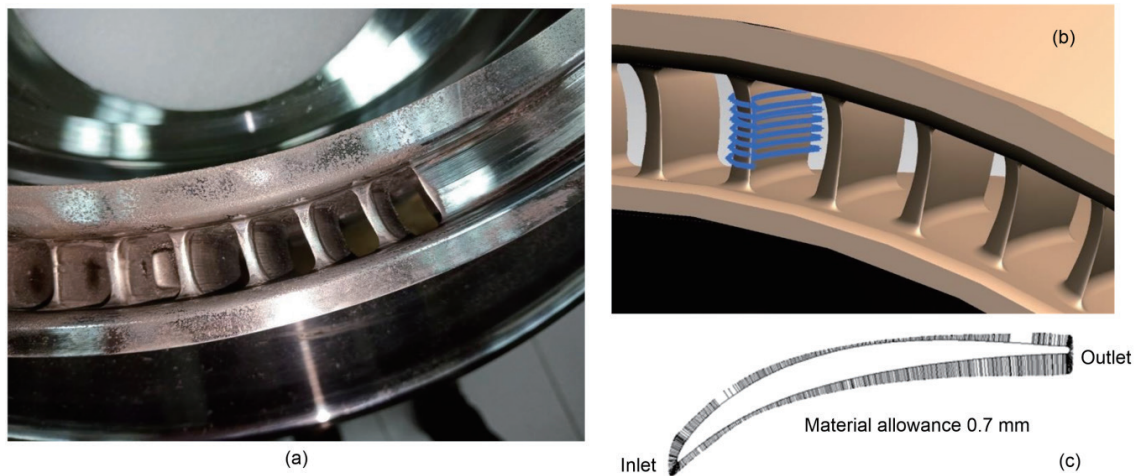
Fig. 4.   (Color online) (a) The diffusion groove is processed and tested under the ECM-optimized electrode, (b) the 3D measurement of diffusion groove processing, and (c) material allowance.

Figure 4(a) shows a trial processing of the optimized electrode on the Inconel 718 plus diffusion tank. Under the processing voltage of 18 V, the electrode feed speed of 15 μm/s, the electrolyte pressure of 3 kgf/cm², and continuous processing for 17 h, the electrode weight before and after processing was reduced by 64 mg. There was no apparent damage to the electrode surface after processing. It is speculated that the weight loss may be due to the decrease in the thickness of the insulation film and the loss of the internal and external burrs of the electrode. This optimized electrode also passed a 17 h processing test using the material SUS304, and there was no apparent damage to the electrode surface in the early stage of electrode optimization. The lifespan of SUS304 does not exceed 3 h, mainly because the flow field is blocked by the products, causing short-circuit discharge during the processing and shortening of the service life of the electrode. Therefore, before and after electrode optimization, the service life of the electrode is considerably improved. The diffusion groove was measured in 3D according to the measurement position specified by the manufacturer and tested under the ECM-optimized electrode, as shown in Fig. 4(b). Figure 4(c) shows a measured section in a 2D manner. After comparing the measured points (the number of samples for a single section is about 180 points) with the finished picture of the diffusion tank, the average of ECM after calculation error is about 0.7 mm. In the ECM method, the electrodes and workpiece are immersed in electrolyte. The workpiece material is connected to the positive electrode, the tool electrode is connected to the negative electrode, and a DC continuous or pulse voltage is applied between the two electrodes. The applied working voltage causes the positive and negative ions in the electrolyte to flow to the positive and negative electrodes, causing oxidation and reduction and then dissolving the anode material.[44] Reality indicates that voltage and current are closely related to processing quality. ECM has many advantages: it is not affected by mechanical stress, has excellent performance without the effect of thermal stress, and has unique processing characteristics due to material hardness and brittleness, especially with almost no tool loss.[45] ECM tools still have advantages in processing, but ECM is complex and challenging to use to

control accuracy. Because of this, how to monitor its quality has become a significant issue. Furthermore, feedback on the quality of ECM compensation in EDM and its structure is shown in Fig. 5.

An experimental parameter is designed to establish the compensation model, the voltage (V) is fixed, and the feed (Fr) condition is changed. The raw data collected from five experiments are shown in Table 1. As the probability of follow-up increases, the current increases, and the processing time shortens.

The workpiece dimensions measured five times on a 3D machine are summarized in Table 1. As shown in the result, the behavior trends of test 1 are relatively different, so only the results of tests 2–5 are included to build the model. Since the EDM discussion focuses on the contact area, the measured area is used for subsequent model building.

An experimental parameter is designed to establish the compensation model, the voltage (V) is fixed, and the feed (Fr) condition is changed. The raw data collected from five experiments are presented in Fig. 6. The probability of follow-up increases, the current increases, and the processing time shortens.
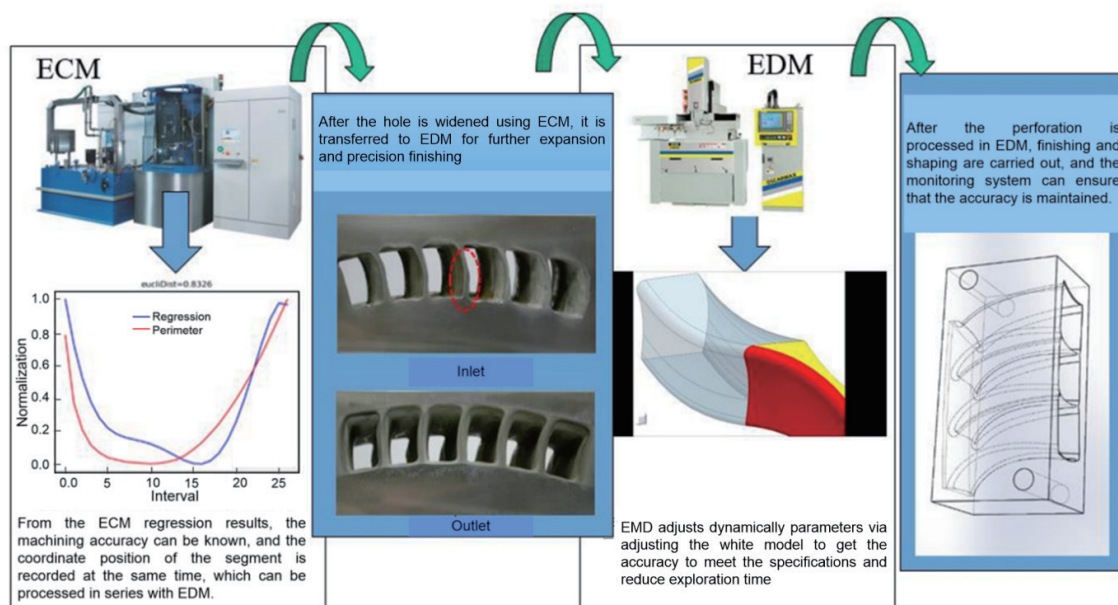

Fig. 5.   (Color online) ECM compensation discharge machining flow chart.

Table 1
Workpiece dimensions on a 3D machine.

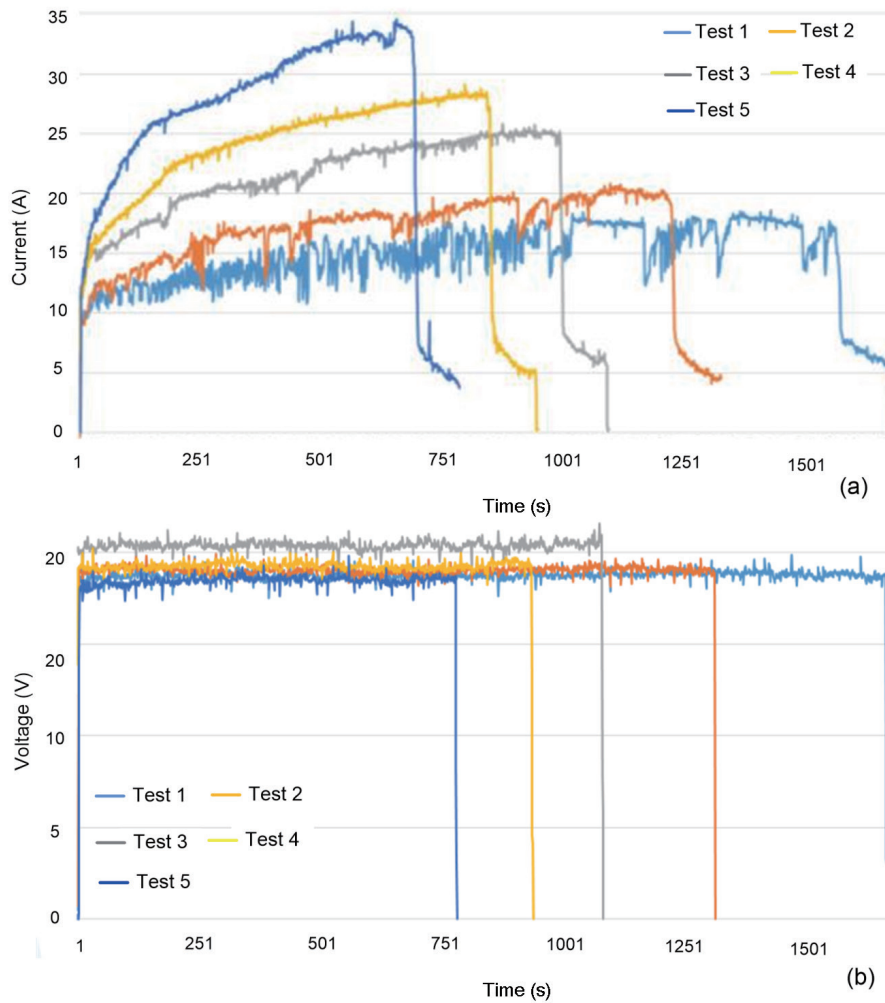|	Test 1 (mm^2)	Test 2 (mm^2)	Test 3 (mm^2)	Test 4 (mm^2)	Test 5 (mm^2)
Tier 1	186.737	184.648	182.246	182.633	179.452
Tier 2	174.828	170.764	167.566	167.369	163.481
Tier 3	173.274	162.794	166.293	166.121	169.486
Tier 4	167.916	168.147	165.297	165.208	161.791
Tier 5	165.757	169.146	167.441	167.067	164.066
Tier 6	171.004	168.132	164.518	164.154	161.284

Fig. 6.   (Color online) Raw data of ECM: (a) voltage and (b) current.

When connecting the two processes, the measurement results of the sixth layer are used for comparison. Owing to the different design areas, the contact areas are different. As shown in Fig. 7, an electrical machining (ECM + EDM) matching method is developed. The machining accuracy is maintained by connecting the rough and postprocessing finishing processes, shortening the process connection processing time, analyzing the correlation across processes, and achieving process matching using electrical signals and removal area calculation mechanisms.

Figure 8(a) shows the correlation among voltage, current, and area at postprocessing measurement values by assigning a score from −1 to 1 to each variable. The result shows that the current and area have an extremely high compatibility, whereas the voltage with current and area show poor compatibility. Figure 8(b) shows the heat map analysis of voltage and current dimensions. The heat map uses a pair plot to analyze the distribution relationship between the two, showing all distributions between variables. Figure 8(b) also shows that the current and size are linear (green box), while the voltage and size (red box) are grouped.

Area removed after ECM processing

	Tier 1	Tier 2	Tier 3	Tier 4	Tier 5	Tier 6
test 2	184.648	170.764	169.486	168.147	169.146	168.132
test 3	182.246	167.566	166.121	165.297	167.441	164.518
test 4	182.633	167.369	166.293	165.208	167.067	164.154
test5	179.452	163.481	162.794	161.791	164.066	161.284

(a)

Area removed after EDM processing

	Tier 1	Tier 2	Tier 3	Tier 4	Tier 5	Tier 6
test 2	189.263	186.526	187.072	187.219	187.171	187.569
test 3	188.54	186.898	187.802	188.012	187.781	188.109
test 4	188.279	186.977	187.834	188.029	187.825	188.074
test 5	187.491	187.164	187.965	188.163	187.98	188.206

(b)

(c)

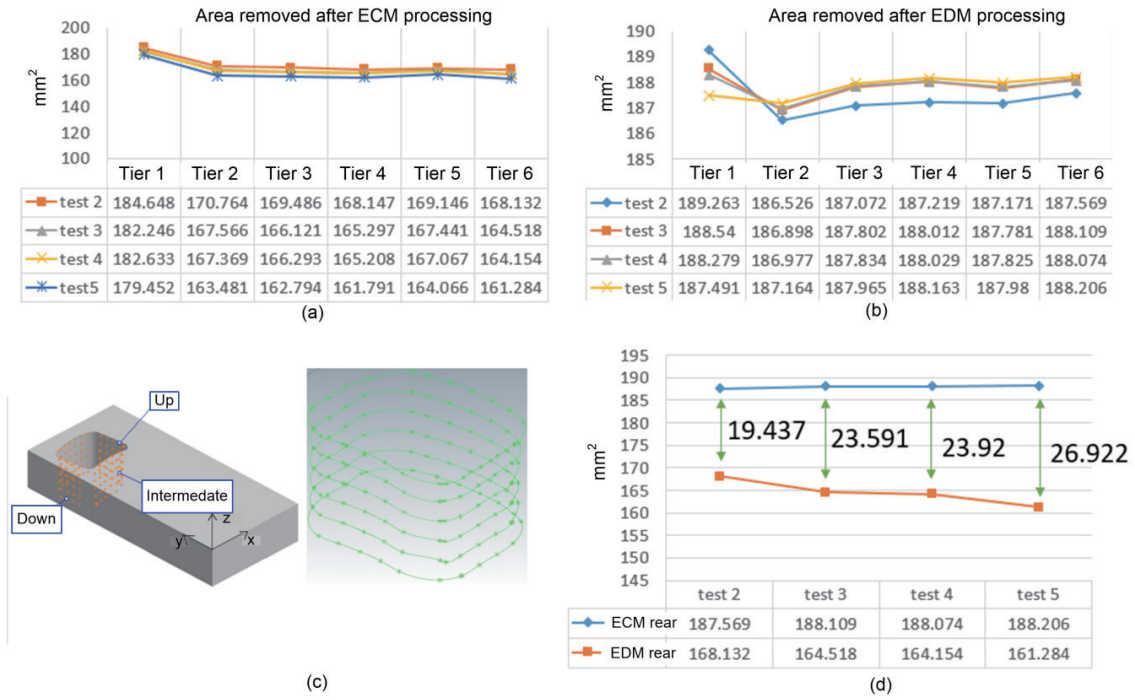|	test 2	test 3	test 4	test 5
ECM rear	187.569	188.109	188.074	188.206
EDM rear	168.132	164.518	164.154	161.284

(d)

Fig. 7.   (Color online) Connection measurement between two processes. (c) The current and size are linear (green box), whereas the voltage and size (red box) are grouped.
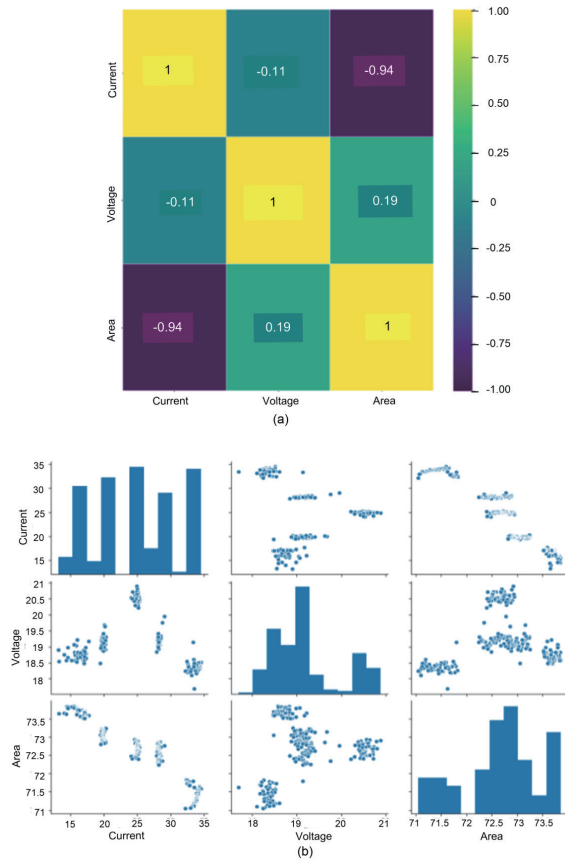

(a)

(b)

Fig. 8.   (Color online) Heat map analysis of voltage and current dimensions: (a) variable distribution relationship analysis and (b) voltage and current size distribution analysis.

We calculated the size change (Δ_{Area}) of the tool inlet and outlet, as shown in Fig. 9(a). The results are that the Δ_{Area} of test 1 is the smallest and that of test 4 is the largest. Figure 9(b) indicates that Δ_{Area} and F_r have a concurrent relationship with time (T), where *Area* (outlet) = $f(V, I)$, then *Area* (inlet) = $f(V, I) \times c$, and *c* is the gradient variable.

The total number of samples is 200, and the model is implemented with 90% (20) random cuts. The mean absolute error (*MAE*) is used to evaluate the difference between the regression results and the actual situation. If there is no difference between the two, the *MAE* is 0. The linear regression model results are shown in Fig. 10. After the test, six points are cut out according to the proportion and compared with the actual value, as shown in Fig. 11. The statistical table shows actual measurements and predictions. The error between points in a single layer is expressed as *MAE*. As shown in Fig. 11, the minimum *MAE* is 0.124 mm^2 for test 2, and the minimum error of a single point is 0.02 mm^2 at the six-floor tier of test 5. Its model can be used for online real-time measurement (monitoring). The processing quality per second can be known and fed back to EDM with "predicted size and time" information to facilitate the series connection of the two processes.

Table 2 shows the surface roughness (*Ra*) values determined by the traditional method (ECM) and our new machining method. The Ra value in this study is about 0.5 μm, which is smaller than those determined in previous studies.[43,46,47]
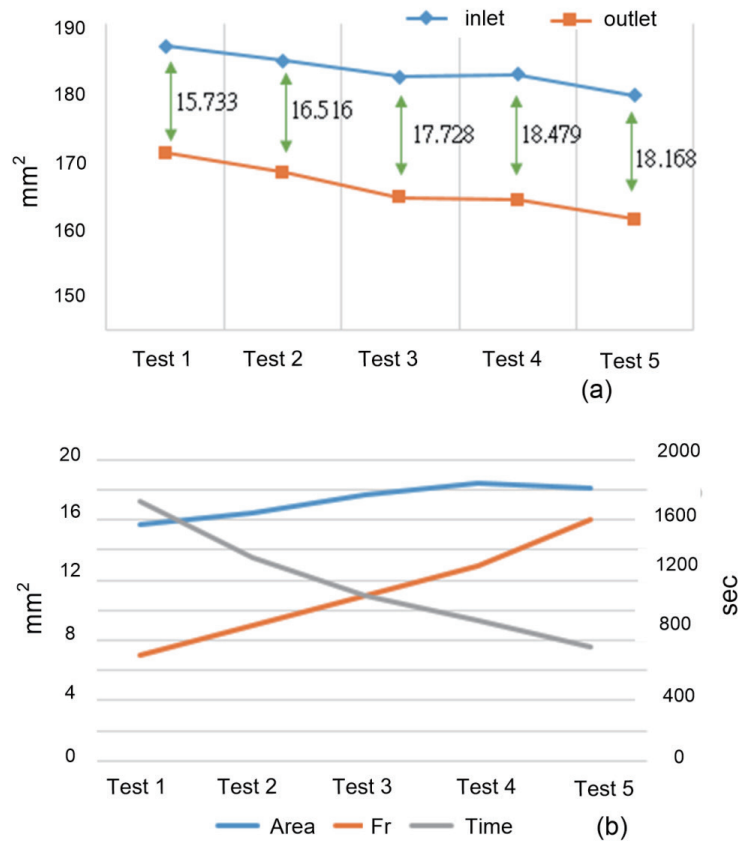

Fig. 9.   (Color online) Analysis of dimensional change: (a) dimensional change and (b) relationship between dimensional change and time.
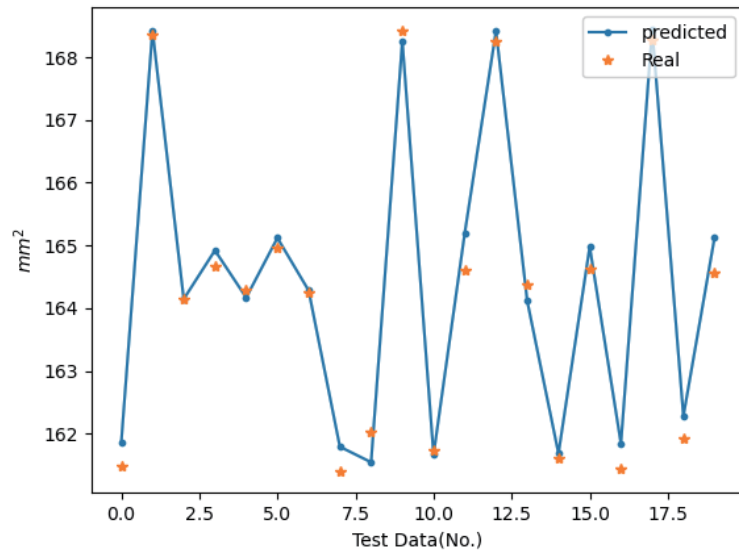
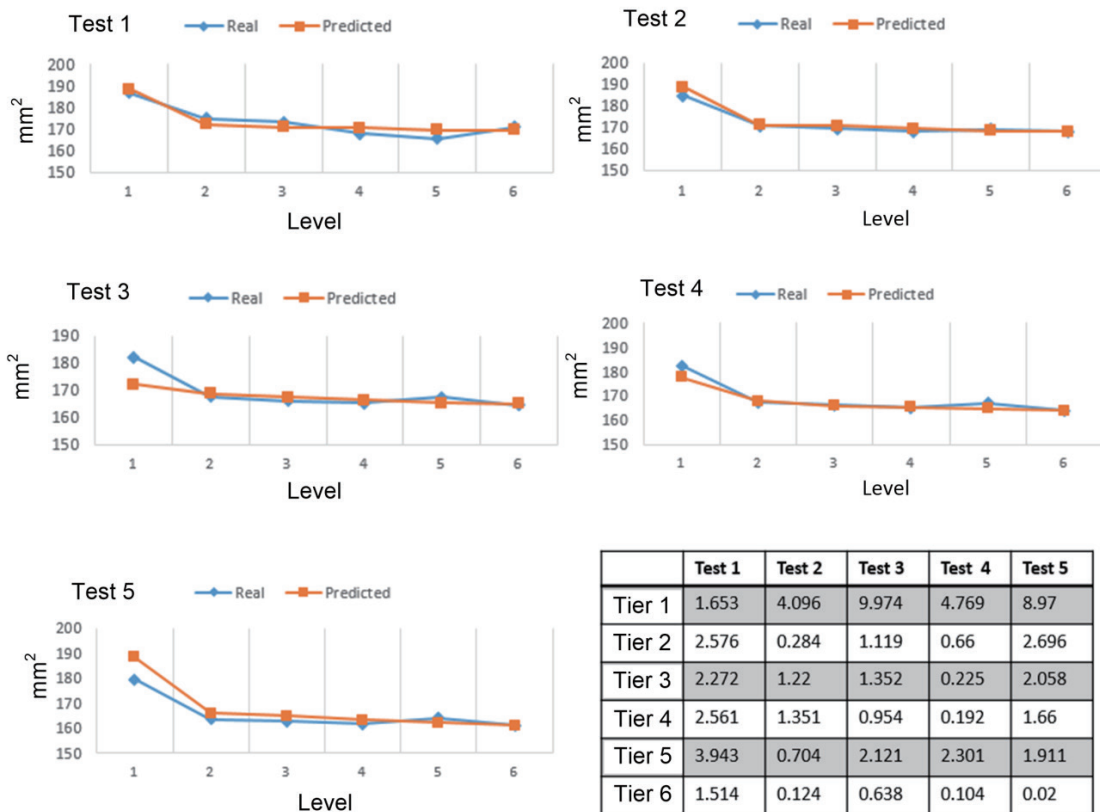Fig. 10.   (Color online) Linear regression model results.

Fig. 11.   (Color online) Actual measurements and model results.

Table 2
Ra values of some machining methods.

Method	Surface roughness (*Ra*) (µm)	References
ECM	2.0–2.5	Asokan *et al.*[46]
ECM	2.0–3.0	Skrabalak *et al.*[43]
ECM	0.6–3.0	Kozak and Zybura-Skrabalak[47]
Novel machining method	0.5	This study

4. Conclusions

In this study, we have completed the establishment of the electrical machining (ECM + EDM) matching method, maintained the machining accuracy of the rough and finishing process, shortened the process connection processing time, and analyzed their correlation across processes using electrical signals and removal area calculation mechanisms to achieve process matching. Moreover, the contact area and time information can be fed back to EDM to facilitate the series connection of the two processes. We also completed the sensor installation and signal acquisition of the EDM process, established the monitoring module for the feature extraction of voltage and current signals, and established an equivalent area estimation model of the actual product. Some vital results are listed below.

After continuous processing for 17 h, the special-shaped hole ECM electrode consumption is ≤10%. The electrical machining line sensing mold with processing accuracy control during discharge is ≤±0.5 µm, and the processing time of the rough/medium machining process is less than 24 h, which is an increase of ≥40%.

The electrode correction estimation model has an equivalent area estimation function with the processing analysis accuracy of more than 80%, the discharge electrode consumption estimation error of smaller than 15%, and the identification speed of only 10 min. The electrical machining process optimization improved the aerospace diffuser processing efficiency by 30%.

Acknowledgments

References

1   L. Zhao, K. C. Chan, S. H. Chen, S. D. Feng, D. X. Han, and G. Wang: Acta Mater. **169** (2019) 122. https://doi.org/10.1038/s41467-019-08722-z
2   S. Guo, D. Xu, Y. Li, Y. Guo, S. Wang, and D. D. Macdonald: J. Supercrit. Fluids **170** (2021) 105138. https://doi.org/10.1016/j.supflu.2020.105138
3   R. Norling and I. Olefjord: Wear **254** (2003) 173. https://doi.org/10.1016/S0043-1648(02)00299-5
4   T. X. Bui, T. H. Fang, and C.-I. Lee: J. Alloys Compd. **924** (2022) 166525. https://doi.org/10.1016/j.jallcom.2022.166525
5   T.-X. Bui, Y.-S. Lu, and T.-H. Fang: Today Commun. **38** (2024) 107795. https://doi.org/10.1016/j.mtcomm.2023.107795

6   W. H Wang, C. Dong, and C. H. Shek: Mater. Sci. Eng. R Rep. **44** (2004) 45. https://doi.org/10.1016/j.mser.2004.03.001

7   P. Vijayakumar, S. Raja, M. A. Rusho, and G. L. Balaji: J. Braz. Soc. Mech. Sci. Eng. **46** (2024) 356.

8   G. Gudivada and A. K. Pandey: J. Alloys Compd. **963** (2023) 171128. https://doi.org/10.1016/j.jallcom.2023.171128

9   T. X. Bui, T. H. Fang, and C. I. Lee: Physica B Condens. Matter. **15** (2020) 412021. https://doi.org/10.1016/j.physb.2020.412021

10 I. G. Akande, O. O. Oluwole, O. S. I. Fayomi, and O. A. Odunlami: Mater. Today: Proc. **43** (2021) 2222. https://doi.org/10.1016/j.matpr.2020.12.523

11 J. Gao, Y. Tong, H. Zhang, L. Zhu, Q. Hu, J. Hu, and S. Zhang: Mater. Charact. **198** (2023) 112740. https://doi.org/10.1016/j.matchar.2023.112740

12 D. Q. Doan, V. H. Nguyen, T. V. Tran, and M. T. Hoang: J. Manuf. Process. **85** (2023) 1010. https://doi.org/10.1016/j.jmapro.2022.12.009

13 C. S. Madigana, A. Vaddula, S. D. Yerramsetti, and K. M. Buddaraju: Materials Today: Proceedings (2023). https://doi.org/10.1016/j.matpr.2023.07.082

14 H. G. Nguyen, T. D. Le, H. G. Nguyen, and T. H. Fang: Mater Sci Eng R: Rep. **160** (2024) 100833. https://doi.org/10.1016/j.mser.2024.100833

15 Y. S. Lu, Y. X. Hung, T. X. Bui, and T. H. Fang: Beilstein J. Nanotechnol. **15** (2024) 925. https://doi.org/10.3762/bjnano.15.76

16 J. Singh and H. S. Gill: Thermal Claddings for Engineering Applications, L. Thakur, J. Singh, and H. Vasudev Eds. (CRC Press, Boca Raton, 2023) 1st ed., Chap. 8. https://doi.org/10.1201/9781032713830-8

17 M. Painuly, R. P. Singh, and R. Trehan: J Solid State Electrochem. **27** (2023) 3189. https://doi.org/10.1007/s10008-023-05610-x

18 S. Kumar, R. Singh, T. P. Singh, and B. L. Sethi: J. Mater. Process. Technol. **209** (2009) 3675. https://doi.org/10.1016/j.jmatprotec.2008.09.032

19 Y. Xing, Y. Yin, F. Wei, X. Ma, S. Zang, J. Zhang, S. Pan, and X. Yue: Int. J. Adv. Manuf. Technol. **133** (2024) 791. https://doi.org/10.1007/s00170-024-13758-7

20 S. Zhang, J. Zhou, G. Hu, L. Wang, and Y. Xu: Int. J. Adv. Manuf. Technol. **129** (2023) 1933. https://doi.org/10.1007/s00170-023-12452-4

21 W. U. Hanqiang, Y. E. Ximin, L. Zhichen, L. I. Sisi, X. Chen, Z. Jiang, S. Zhang, and W. U. Yongbo: Chin. J. Aeronaut. (2024). https://doi.org/10.1016/j.cja.2024.07.002

22 M. Singh and S. Singh: J. Adv. Manuf. Technol: Selected Extended Papers of ICAMMS (2018) 139. https://doi.org/10.1007/978-3-319-76276-0_14

23 J. Kozak and M. Zybura-Skrabalak: Procedia Cirp. **42** (2016) 101. https://doi.org/10.1016/j.procir.2016.02.198

24 S. Boopathi, A. S. Alqahtani, A. Mubarakali, and P. Panchatcharam: Environ. Sci. Pollut. Res. **31** (2024) 38940. https://doi.org/10.1007/s11356-023-27494-0

25 M. Manikandan, S. Arun, B. Kuriachen, and J. Mathew: Mater. Today Proc. (2023). https://doi.org/10.1016/j.matpr.2023.07.139

26 H. Dong, W. Gong, Y. Qiu, and J. Zhou: Int. J. Adv. Manuf. Technol. **130** (2024) 799. https://doi.org/10.1007/s00170-023-12750-x

27 W. Ming, S. Zhang, G. Zhang, J. Du, J. Ma, W. He, C. Cao, and K. Liu: Int. J. Heat Mass Transf. **187** (2022) 122563. https://doi.org/10.1016/j.ijheatmasstransfer.2022.122563

28 M. Sana, M. Asad, M. U. Farooq, S. Anwar, and M. Talha: Int. J. Adv. Manuf. Technol. **130** (2024) 5641. https://doi.org/10.1007/s00170-024-13023-x

29 X. Wu, Y. Liu, P. Zhang, C. Zheng, Y. Han, D. Li, R. Bian, and R. Ji: J. Clean. Prod. **452** (2024) 142150. https://doi.org/10.1016/j.jclepro.2024.142150

30 Q. Li and X. Yang: Precis. Eng. **85** (2024) 126. https://doi.org/10.1016/j.precisioneng.2023.09.013

31 S. Chen, H. Gu, J. Wang, W. Chang, and K. Chan: Int. J. Adv. Manuf. Technol. **126** (2023) 5057. https://doi.org/10.1007/s00170-023-11459-1

32 M. A. Karim and M. P. Jahan: J. Manuf. Process. (2024) 171. https://doi.org/10.1016/B978-0-323-95318-4.00007-0

33 L. Qin, W. Huo, Z. Li, Y. Zhang, X. Xi, and W. Zhao: Int. J. Adv. Manuf. Technol. **121** (2022) 5563. https://doi.org/10.1007/s00170-022-09755-3

34 M. Xu, C. Li, R. Kurniawan, J. Chen, and T. J. Ko: Int. J. Precis. Eng. Manuf. **23** (2022) 1095. https://doi.org/10.1007/s12541-022-00689-0

35 K. Surani, S. Patel, A. J. Alrubaie, A. Oza, H. Panchal, S. Kumar, and S. Zahmatkesh: Int. J. Interact. Des. Manuf. **17** (2023) 2647. https://doi.org/10.1007/s12008-022-01088-5

36 N. Alharbi: Arab. J. Sci. Eng. **47** (2022) 15661. https://doi.org/10.1007/s13369-022-06713-9

37 S. Boopathi, A. S. Alqahtani, A. Mubarakali, and P. Panchatcharam: Sci. Pollut. Res. **31** (2024) 38940. https://doi.org/10.1007/s11356-023-27494-0

38 S. Boopathi: Environ. Sci. Pollut. Res. Int. **29** (2022) 86237. https://doi.org/10.1007/s11356-021-17658-1

39 S. Boopathi, A. S. Alqahtani, A. Mubarakali, and P. Panchatcharam: Environ. Sci. Pollut. Res. **31** (2024) 38940. https://doi.org/10.1007/s11356-023-27494-0

40 K. Gunasekaran, S. Boopathi, and M. Sureshkumar: Mater. Technol. **56** (2022) 179. https://doi.org/10.17222/mit.2022.397

41 V. K. Yadav, R. Singh, P. Kumar, and A. Dvivedi: J. Mater. Eng. Perform. **31** (2022) 8405. https://doi.org/10.1007/s11665-022-06811-7

42 M.S. Shah, D. Gupta, P. Saha, A. Assam, and C. Sarkar: Int. J. Adv. Manuf. Technol. **127** (2023) 775. https://doi.org/10.1007/s00170-023-11594-9

43 G. Skrabalak, M. Zybura-Skrabalak, and A. Ruszaj: J. Mater. Process. Technol. **149** (2004) 530. https://doi.org/10.1016/j.jmatprotec.2003.11.058

44 R. J. Leese and A. Ivanov: Adv. Mech. Eng. **8** (2016). https://doi.org/10.1177/1687814015626860

45 M. A. H. Mithu, G. Fantoni, and J. Ciampi: Int. J. Adv. Manuf. Technol. **55** (2011) 921. https://doi.org/10.1007/s00170-010-3123-3

46 P. Asokan, R. Ravi Kumar, R. Jeyapaul, and M. Santhi: Int. J. Adv. Manuf. Technol. **39** (2008) 55. https://doi.org/10.1007/s00170-007-1204-8

47 J. Kozak and M. Zybura-Skrabalak: Procedia Cirp. **42** (2016) 101. https://doi.org/10.1016/j.procir.2016.02.198